PHYSICAL REVIEW D **93,** 053013 (2016)

# Distinguishing $b$-quark and gluon jets with a tagged $b$ hadron

Dorival Gonçalves, Frank Krauss, and Robin Linten
*Institute for Particle Physics Phenomenology Physics Department, Durham University Durham DH1 3LE, United Kingdom*
(Received 11 January 2016; published 18 March 2016)

Based on the knowledge of the QCD radiation pattern, observables to distinguish jets containing one and two $b$ hadrons are discussed. A simple method is used to combine pairs of the most sensitive observables—girth, number of charged tracks and the energy or momentum fraction of the leading $b$ hadron with respect to the jet—into one discriminator. Their efficiencies, on the particle level, are estimated and found to improve the performance and the robustness of the observables in different momentum slices.

DOI: 10.1103/PhysRevD.93.053013

## I. INTRODUCTION

Jets containing a bottom quark play a significant role in many analyses at the LHC, both in searches for new physics and in further studies of the Standard Model. As an illustrative example, consider the measurements of the phenomenologically relevant Yukawa couplings of the newly found Higgs boson to quarks of the third-generation top and bottom quarks. One of the processes central to this measurement is the production of a Higgs boson in association with top quarks, $pp \to t\bar{t}H$, where the Higgs boson decays into a $b\bar{b}$ pair. For this study, both the signal and the dominant background processes are understood at next-to-leading order (NLO) in QCD [1–6]. More modern fixed-order calculations, performed with automated tools such as OpenLoops+Sherpa [7–9] or MadGraph5 [10,11], have successfully been embedded in hadron-level simulations based on Mc@Nlo [12], for the signal process $t\bar{t}H$ [13], and the dominant irreducible background $t\bar{t}b\bar{b}$ [14]. Multijet merging technologies at NLO [15–18] have successfully been applied to the production of top-antitop pairs in conjunction with jets [19,20], thereby also providing a handle on this background. Combined, this work represents an amazing technological development. However, looking at the analysis strategy employed by both ATLAS and CMS, it becomes clear that the experimental cuts shape the background and the signal to look relatively similar, rendering them hard to distinguish. In the end, it essentially reduces this analysis to the counting of events with a suitable number of $b$ jets—three or four—within certain acceptance regions [21–24].

One of the problems arising from this kind of analysis is related to the fact that they rely on the identification of $b$ quarks through jets with a $b$ tag. This identification is realized by $b$-tagging conditions [25–27]. Examples include criteria based on displaced vertices with a certain impact parameter significance, the presence of soft muons inside the jet, which may stem from such a displaced vertex, or criteria based on the further decay chain and their possible impact on the intrinsic shape of such tagged jet [28]. Usually, the acceptance rate of jets including a $b$ hadron based on such tags is relatively high, between 60% and 70%, while the rejection rate of light jets containing no such hadron reaches well beyond 90% at typical working points. However, this simple tagging technology may fail to reliably identify jets containing two $b$ hadrons, which can originate from a $g \to b\bar{b}$ splitting. This translates into limitations in distinguishing "legitimate" $b$ jets stemming from a $b$ quark from gluon (or other light) jets, thereby hampering analyses of processes with $b$'s produced in the hard interaction. This is further exacerbated by the absence of very precise theory estimates of the gluon splitting: its description by the parton shower is possibly not quite as reliable as one would naively assume. Earlier analyses by the LEP Collaborations measured this splitting probability with large statistical and systematic errors in the range of $(0.21\% - 0.31\%) \pm 0.1\%$, while the parton shower programs usually arrived at rates of just below 0.2% [29–32]. This immediately translates into the need to measure the $g \to b\bar{b}$ transition such that the modern parton shower algorithms can be compared and, if necessary, improved through direct comparison. It also motivates us to construct robust and reliable observables discriminating the "real" $b$ jets from those jets where a $b\bar{b}$ pair emerges from gluon splitting.

Some early attempts at this identification were performed by CDF [33] by trying to identify two secondary vertices in the jet consistent with two $b$ hadrons from a sample of already tagged events. Both ATLAS [34] and CMS [35] are also working on this identification, with varying levels of success. Due to the intrinsic difficulty of finding two separate secondary vertices belonging to $b$ hadrons, these searches are typically using observables related to the jet and the vertex. Both collaborations use sophisticated multivariate analysis tools to define their discriminators.

This short paper aims to further explore the very same problem. Using well-established features in the QCD radiation pattern and simple geometric considerations

 

motivates us to use a combination of jet shapes and a secondary vertex finding to distinguish $b$ jets from what will be called $b\bar{b}$ jets in the rest of the paper. This paper is organized as follows: In Sec. II, the most sensitive jet shape observables are reviewed, and possible improvements when combining them with a reconstruction of fragmentation function observables are discussed. Since the last observable is a new discriminant in the context of single vs double $b$-tag jets, we devote special emphasis to it. The analysis is performed in Sec. III, the results presented in Sec. IV, and the summary in Sec. V.

## II. SHAPING $b$ JETS: KINEMATIC OBSERVABLES

It is well known that the fragmentation function $F(x)$ of $b$ quarks is relatively hard, peaking close to $x \approx 1$. Here, $x$ denotes the $b$-hadron energy or momentum fractions $x_E$ or $x_p$ with respect to the underlying $b$-quark jet. This behavior is due to the fact that the finite masses of the $b$ quarks shield the collinear divergence in gluon emissions off the quark, thereby effectively suppressing the emission of energetic secondary partons, a phenomenon sometimes called the "dead cone effect." As a result, $b$ quarks tend to retain most of their energy—in contrast to light partons—and thus the $b$ hadrons more or less have energies and momenta very similar to the $b$ quark when it was produced in the hard process. Conversely, $b$ quarks originating from a gluon splitting tend to have a fairly symmetric share in the energy of the original gluon, which they retain during fragmentation. As a result, the emerging $b$ hadrons, and in particular also the harder of the two, tend to have an energy fraction well below unity.

A somewhat independent observable is related to the shape of the actual jet. Based on the reasoning above, $b$ jets tend to be relatively narrow, with only small amounts of radiation roughly following the direction of the color connection of the $b$ quark to the rest of the event. In contrast, $b\bar{b}$ jets tend to originate from hard gluons, which may not only radiate more due to the larger color charge of $C_A = 3$ vs $C_F = 4/3$ before they split, but which also have an intrinsic size related to the relative distance of the two $b$ quarks inside the jet. This effect could be captured by using the mean of the energy distribution $\rho(r)$ inside the jet, where $r < R$ is the radial distance of a hadron or similar to the centroid of the jet with radius $R$. It turns out, however, that a good observable is provided by the first $p_\perp$ moment of this distribution,

$$g = \frac{1}{p_\perp^{(J)}} \sum_{i \in \text{Jet}} p_\perp^{(i)} \Delta R_{iJ}, \tag{1}$$

an observable also known as "girth," $g$, or jet width. Here $p_\perp^{(J)}$ is the transverse momentum of the jet, $p_\perp^{(i)}$ the transverse momentum of the hadron, track, or energy cell $(i)$ inside the jet $(i \in \text{Jet})$, and $\Delta R_{iJ}$ is its radial distance with respect to the jet vector.

Many more observables can be used with different distinguishing powers and robustness. A prime example is the number of charged tracks $n_{\text{ch}}$. Despite presenting a possibly poor Monte Carlo modeling, highly depending on the details of hadronization modeling and underlying event implementation, they are still extensively used by experimental analyses. Hence, we also inspect its impact in the following section.

The typical behavior of these observables is exemplified in Fig. 1; in this figure all jets have a transverse momentum $p_\perp^J$ between 50 and 100 GeV and their pseudorapidity $|\eta_J| < 2.5$. To provide an idea of modeling uncertainties, the results of different event generators—HERWIG++ [36], PYTHIA 8 [37] and SHERPA [9]—are exhibited.

There are other observables that aim to scrutinize the color connection and two-dimensional shape of the jet, e.g., planar flow, pull or differential jet shape that were also inspected. However, in this study only the most powerful observables will be investigated, namely fragmentation fractions $x_E$, girth $g$ and number of charged tracks $n_{\text{ch}}$.

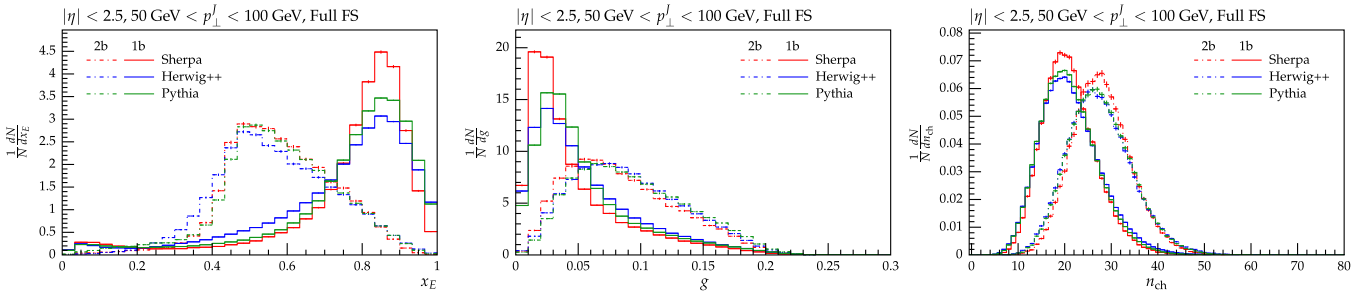


FIG. 1. Comparison of $x_E$, $g$, $n_{\text{ch}}$ from different event generators for jets within 50 GeV $< p_\perp^J <$ 100 GeV, based on the full hadronic final state. The left panel shows results for $x_E$. The little enhancement at small values of $x_E$ stems from light jets, where a single $b$ quark was inserted, either through gluon splitting, where the other $b$ quark was radiated outside the jet, or by the underlying event. The central panel shows results for $g$, where the $b$ hadron(s) were set stable—this was only done in this plot and none of the rest of the paper. The right panel shows the number of final state particles inside the jet (including uncharged ones). A vertex is defined as having at least three tracks.

These additional observables could be used in the construction of more advanced discriminators based on boosted decision trees or neural networks, which is beyond the scope of this study. It is worth noting that there are interesting similarities between the investigations here and studies aiming at distinguishing gluon and light quark jets, see for instance Ref. [38,39]. Due to the somewhat different gluon and light quark fragmentation fraction profiles, for obvious reasons, they present sensibly weaker efficiencies in comparison to the single vs double $b$-tag case.

## III. ANALYSIS

As a test case, a pure QCD $pp \to$ jets sample at the $\sqrt{s} = 13$ TeV LHC is considered. The event sample was generated with SHERPA [9] in a very basic setup, using $2 \to 2$ matrix elements at leading order, supplemented with the default parton shower based on Catani-Seymour subtraction [40], and accounting for hadronization and underlying event effects. Since different event generators differ in their approximations and implementation details of the parton shower evolution and nonperturbative models, it is important to quantify the resulting uncertainties and to access the robustness of the results. To this end, event samples with the same specifications have been generated and analyzed, using HERWIG++ [36] and PYTHIA 8 [37]. Where relevant, the results from these different simulation tools are contrasted; overall, however, they do not impact on the results and conclusions of this study.

The analysis is performed using RIVET [41]. Jets are defined by the anti-$k_T$ algorithm, using FASTJET [42], with $R = 0.4$, requiring $p_\perp^J > 30$ GeV and $|\eta_J| < 2.5$. Charged

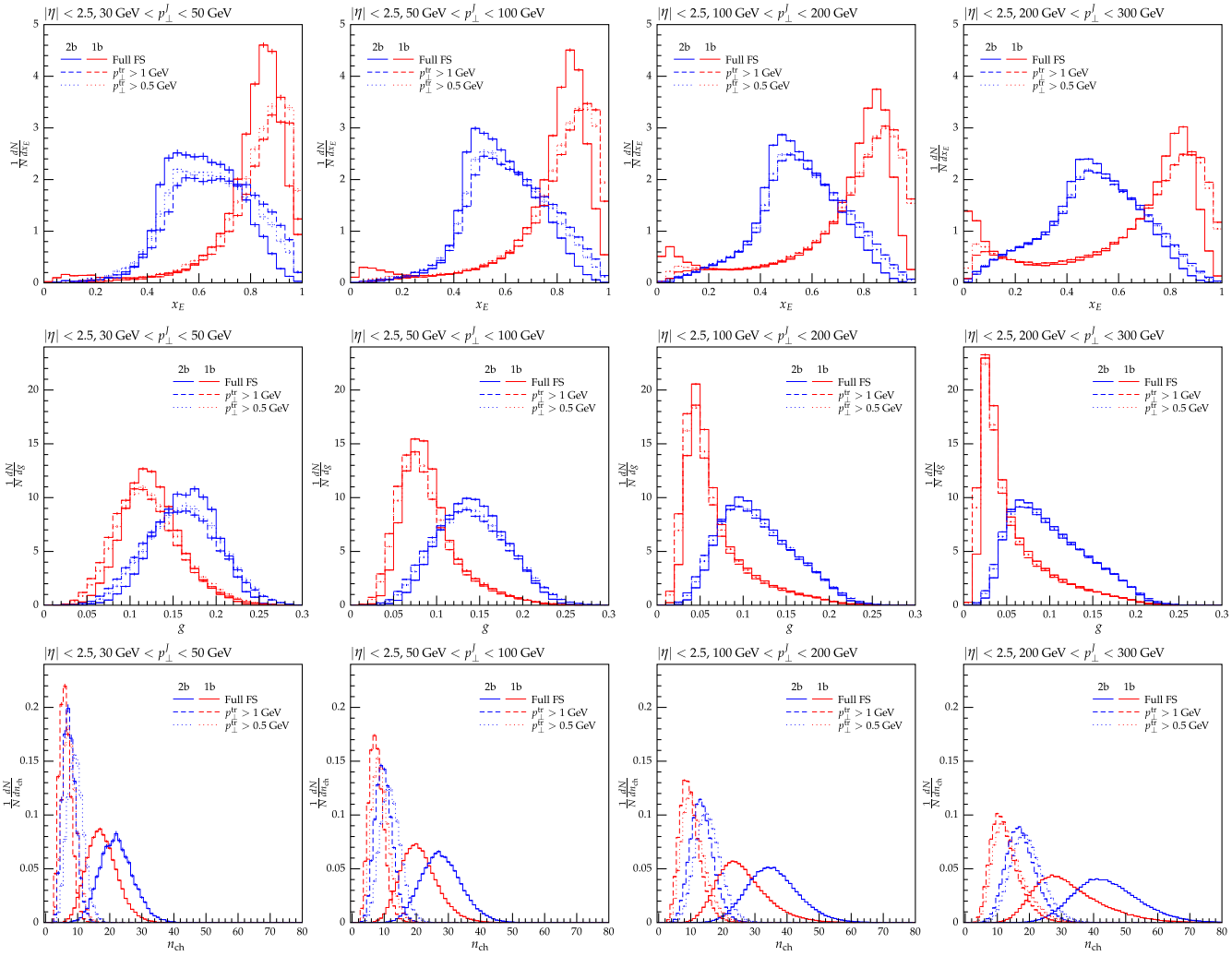


FIG. 2. $x_E$ (top row), girth (central row) and number of charged tracks (bottom row) distributions for jets within different $p_\perp$ slices: 30 GeV $< p_\perp^J <$ 50 GeV (first column) 50 GeV $< p_\perp^J <$ 100 GeV (second column), 100 GeV $< p_\perp^J <$ 200 GeV (third column) and 200 GeV $< p_\perp^J <$ 300 GeV (fourth column). Red curves correspond to jets with one $b$ hadron and blue with two $b$ hadrons. Solid lines are based on the full hadronic final state, including uncharged particles, dashed lines on charged tracks with a minimum $p_\perp^{\rm tr}$ of 1 GeV and dotted with a minimum $p_\perp^{\rm tr}$ of 0.5 GeV. A vertex is defined as having at least three tracks.

tracks are defined with a minimum transverse momentum $p_\perp^{\rm tr} \geq 0.5$ or 1 GeV. The different cutoffs are used to probe the stability of the observables. Lowering the threshold would of course lead to more statistics; however, it also increases the dependence on the MC modeling.

Jets are categorized as containing one or two $b$ hadrons, with other values rejected, counting their number inside the jet radius. For our purposes, the $b$ hadrons are "reconstructed" from the event record, taking into account the choice of observable final state particles. In case of two different $b$ hadrons in the jet, by default the harder one is selected.

In Fig. 2 (top row), the $x_E$ distributions are displayed. It is observed that in the case of one $b$ hadron in the jet, the $b$ hadron carries most of the energy content with the distribution peaking between 0.8 and 1, depending on the $p_\perp$ slice. On the other hand, in the case of two $b$ hadrons in the jet the energy fraction for the most energetic $b$-hadron tend to be near 0.5–0.6. These effects do not diminish when considering only charged tracks; rather, it improves slightly, e.g., the distribution for one $b$ quark in the jet narrows near $x_E = 1$. Similar observables built out of the 3-momentum, the transverse momentum or weighted with the cosine of the angle to the jet axis present qualitatively and quantitatively similarities to $x_E$. Therefore, only the latter is considered for simplicity.

The girth distributions $g$ are displayed in Fig. 2 (central row). This observable presents a good separation between the single and double $b$-tagging case. The double $b$-tag sample leads to broader jets in respect to the single $b$-tag case. This observable presents useful results at either low or high $p_\perp^J$. Moreover, the charged tracks present qualitatively similar results and only a subleading dependence on the threshold energy, $p_\perp^{\rm tr} > 0.5$ GeV or 1 GeV, is observed.

The dependence on the charged track multiplicity $n_{\rm ch}$ is inspected in Fig. 2 (bottom row). The jets with two $b$ hadrons present a much higher multiplicity than the single $b$-tagged. This is a result of the longer decay chain of the $b$ hadron and the different emission pattern described by the parton shower. These differences are enhanced at higher $p_\perp^J$ where the $n_{\rm ch}^{2b}/n_{\rm ch}^{1b}$ slowly converges to $C_A/C_F$.

Despite $n_{\rm ch}$ not being an infrared safe observable and therefore highly dependent on the parton shower, hadronization and underlying event modeling, the disagreement with the MCs is usually suppressed via an appropriate tuning to the LHC data. Hence, its applications have to account for these limitations and/or should be taken with a grain of salt.

Notice that in the boosted kinematics, the $x_E$ distribution displays an enhancement at low $x_E$ for the single $b$-hadron jet, see Fig. 2 (top-right panel). Again, QCD radiation in the form of $g \to b\bar{b}$ splittings, accounts for the observed feature. It appears in the boosted regime because the larger initial energy of the jets leads to an enhanced emission phase space with more gluons being produced during the perturbative part of their fragmentation. This is exemplified by two $x_E - \Delta R_{bb}$ correlation plots, in Fig. 3. The two plots correlate the $x_E$ of the $b$ hadrons inside single-$b$-tagged tagged jets with their spatial distance $\Delta R_{bb}$ with respect to the other $b$ hadron, outside the jet. In the left panel, for low transverse momentum jets with 30 GeV $\leq p_\perp \leq$ 50 GeV, the other $b$ has a typical distance of $\Delta R_{bb} \gtrsim 0.5$, and the $b$ tag inside the jet resides at $x_E$ values around 0.8 or so. In the right panel, referring to the highly boosted regime, with 200 GeV $\leq p_\perp \leq$ 300 GeV a second hot spot in the correlation plot emerges, for low values of $x_E$ close to 0, and the $\Delta R_{bb}$ distance becomes smaller than 0.4, indicating that in this case the $b$ tags reside closer to the jet boundary. This suggests that these $b$ hadrons "leaked" into a hard, light jet. In fact, such $b$ tags should therefore probably not be identified with "legitimate" $b$ jets originating from a primary hard $b$ quark.

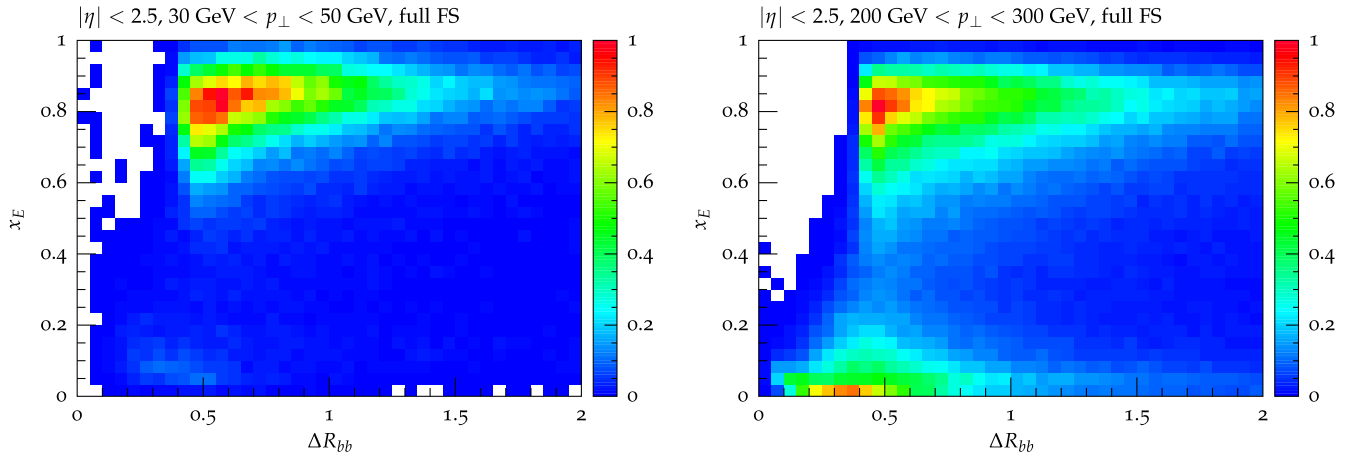


FIG. 3. Normalized $(x_E, \Delta R_{bb})$ distributions for the one $b$-hadron jet. The jets are considered in two momentum slices: $p_\perp^J$ of 30 to 50 GeV (left panel) and $p_\perp^J$ of 200 to 300 GeV (right panel). The results here are based on fully hadronic final states.

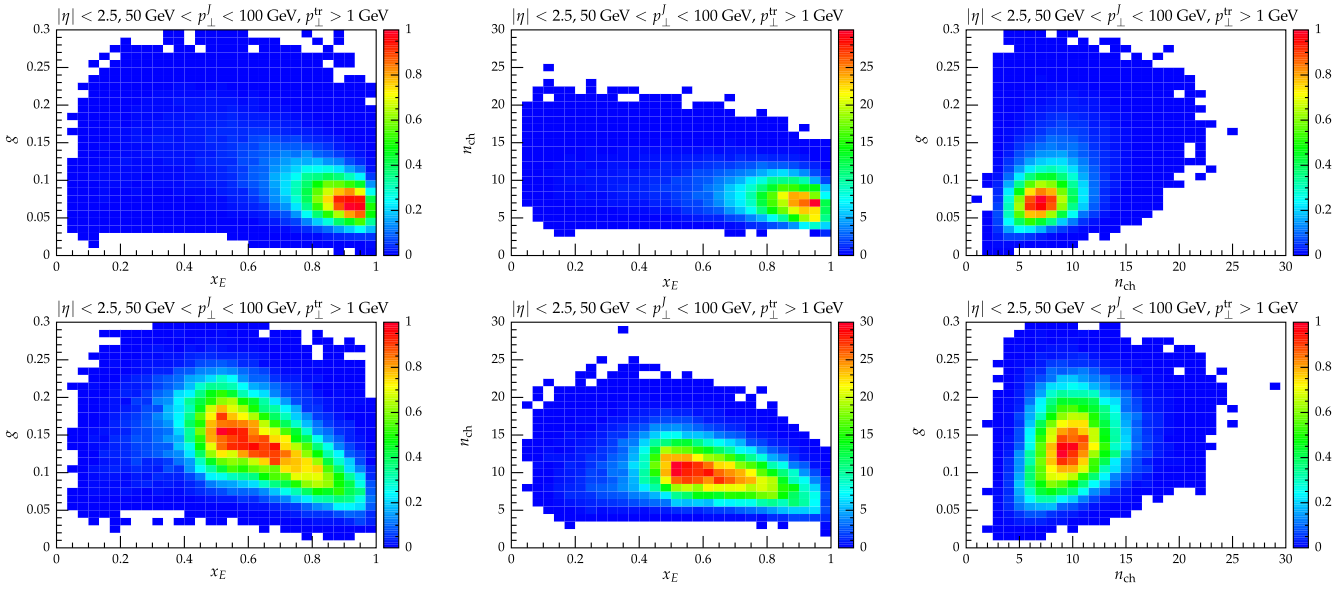


FIG. 4. Correlations between the fragmentation fraction with the girth $(x_E, g)$ (left column), fragmentation fraction with charged tracks $(x_E, n_{ch})$ (central column) and charged tracks with girth $(g, n_{ch})$ (right column). The colors represent the normalized weight of the particular bin. The top plots are for one $b$ hadron in the jet, the bottom ones for two $b$ hadrons in the jet. The jets considered here have a $p_\perp^J$ of 50 to 100 GeV. The objects considered in the analysis in this case are charged tracks of at least 1 GeV $p_\perp^{tr}$. A vertex is defined as having at least three tracks.

## IV. DOUBLE AND SINGLE $b$-TAGGING EFFICIENCIES

The observables $x_E$, $g$ and $n_{ch}$ provide good sensitivity towards the single and double $b$-tagging samples when considered independently. As most of the $b$-tagging algorithms resort to multivariate analysis (MVA) with the combination of the most significative distributions, it is important to assure that these observables do not present the same correlation pattern and could therefore generate improved constraints through their combination. In Fig. 4, the two-dimensional correlations between the fragmentation fraction, girth and charged track multiplicity are displayed, showing only the case for charged tracks of $p_\perp^{tr} > 1$ GeV for jets in the $p_\perp^J$-bin between 50 and 100 GeV. The behavior seen in these plots is qualitatively observed also for higher transverse momenta.

Tagging efficiencies are defined based on the so-called ROC curve that uses a simple cut argument. For the one-dimensional distributions, as shown in Fig. 2, the efficiency curve is obtained by sliding a cut along the value of the observable. Each point of the cut leads to a correspondent efficiency for keeping $b$ jets $(\epsilon_{1b})$ and $b\bar{b}$ jets $(\epsilon_{2b})$. The ROC curve is the interpolation of all possible cuts. For instance, for the girth and multiplicity, a jet is tagged as containing two $b$ hadrons, if the value of the observable is above the cut. Whereas, for the fragmentation fractions it is tagged as such when the observable is below the cut. The efficiency to tag a jet containing one $b$ hadron is defined analogously. The region $x_E < 0.3$ is removed to avoid the lower peak in the boosted regime to maximize the performance of this method. This region could be efficiently included via a MVA, but this was not done in this letter to retain the simplicity of our strategy. The generalization to the combination of two observables is straightforward: Carrying out a principal component analysis on the correlation plots for two $b$ hadrons in the jet, a cut line can be defined perpendicular to the largest eigenvector of the correlation. The jet is tagged as containing two $b$ hadrons if the pair $(x_E, g)$, $(x_E, n_{ch})$ or $(g, n_{ch})$ is above this line. Sliding the cut line along the eigenvector of the correlation matrix, tag and mistag efficiencies can be determined.

These efficiencies are shown in Fig. 5 (top row) as the efficiency of tagging a $b$ jet as a jet containing two $b$ hadrons, $\epsilon_{2b}$, against the rejection of $b$ jets, $1/\bar{\epsilon}_{1b}$. The combination of observables proves to be robust against the choice of charged tracks or the fully hadronic final state. Lowering the threshold $p_\perp^{tr}$ to 0.5 GeV produces only mild improvements in respect to 1 GeV.

In Fig. 5 (bottom row), different combinations of observables are compared with the discrimination from $n_{ch}$ or $x_E$ only. A visible improvement in using the combination of two observables is found. For low transverse momenta the combination $(x_E, g)$ outperforms the other combinations, while for larger transverse momenta of the jet, the combination of $(x_E, n_{ch})$ is most sensitive. In both cases, however, the fragmentation fraction is involved, an observable that hitherto has not been documented for this discrimination.

In Fig. 6, the different combinations are displayed for distinct transverse momenta slices. The $b\bar{b}$-jet rejection

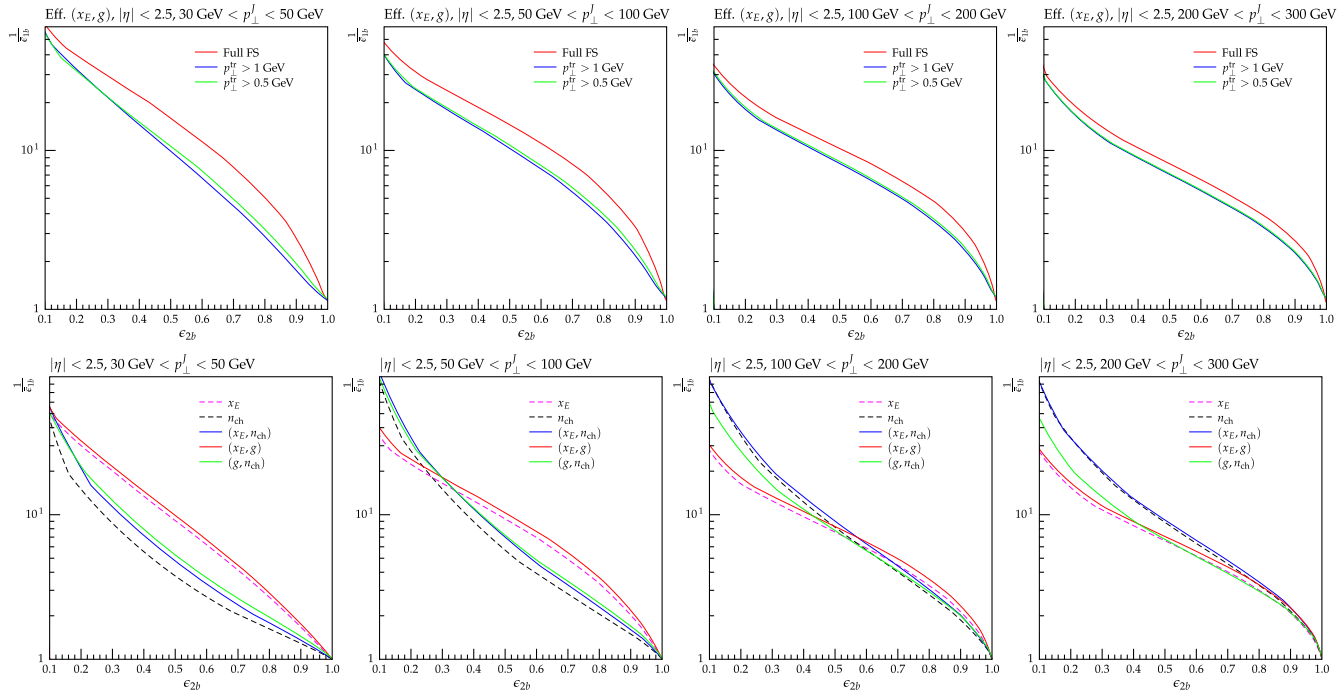


FIG. 5. Efficiency for tagging a $b$-jet as containing two $b$ hadrons $\epsilon_{2b}$ against the rejection of jets containing one $b$ hadron $1/\bar{\epsilon}_{1b}$ from combining $x_E$ and girth. The plots are again shown in different $p_\perp^J$ bins as in Fig. 2. Top row: The red curves refer to an analysis using the full final state, whereas the blue and green consider only charged tracks with minimum $p_\perp^{\rm tr}$ of 1 GeV and 0.5 GeV, respectively. Bottom row: efficiencies for different combinations of observables [red: $(x_E, g)$, blue: $(x_E, n_{\rm ch})$, green: $(g, n_{\rm ch})$]. The displayed results refer to charged tracks with minimum $p_\perp^{\rm tr}$ of 1 GeV.

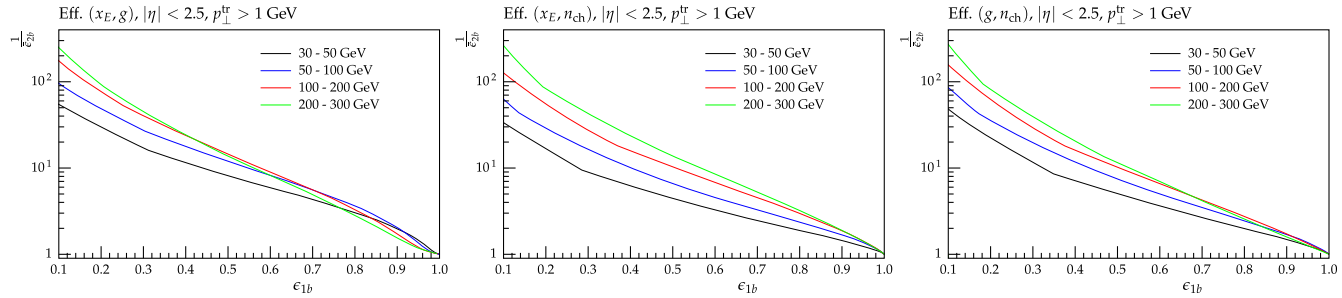


FIG. 6. Efficiency for tagging a $b$ jet as containing one $b$ hadron $\epsilon_{1b}$ against the rejection of jets containing two $b$ hadrons $1/\bar{\epsilon}_{2b}$ as a function of $p_\perp^J$ for different combinations of observables. Left: $(x_E, g)$, center: $(x_E, n_{\rm ch})$, right: $(n_{\rm ch}, g)$.

efficiency $(1/\bar{\epsilon}_{2b})$ significantly improves for these phenomenologically interesting boosted topologies in all cases. The $(x_E, g)$ produces robust results through all the transverse momentum slices. This suggests that the combination of these two observables contains complementary and relevant information not found in the single observables or the other combinations.

## V. SUMMARY

Studies that require multiple $b$ jets will become increasingly frequent at the LHC in the years to come. These studies range from SM precision analyses to searches for beyond the SM physics, such as resonance searches. One of the problems encountered is related to discriminating the "legitimate" $b$ jets, containing only one, typically hard, $b$ hadron, from jets containing two $b$ hadrons, usually emerging from a gluon splitting. In this publication a phenomenological attempt at a more coherent strategy of discriminating $b$ and $b\bar{b}$ jets has been presented, based on possible kinematic handles, in particular combinations of jet shapes with the fragmentation fraction.

Several observables were considered and the most powerful encountered were the girth $g$, the number of charged tracks $n_{\rm ch}$, and $b$-hadron jet energy fraction $x_E$. Especially when combining either of the former two with

the latter a considerable improvement was found. A significant improvement for the $b\bar{b}$-jet rejection is observed at the boosted regime for all variable combinations.

We note in passing that in the boosted regime a sizable fraction of $b$ tags correspond to $b$ hadrons with a low $x_E$, stemming predominantly from the splitting of secondary gluons in the jets. A simple cut on $x_E$ will remove such unwated $b$ tags.

## ACKNOWLEDGMENTS

The authors acknowledge financial support by the UK Science and Technology Facilities Council, by the Research Executive Agency (REA) of the European Union under the Grant Agreements No. PITN-GA-2012-316704 ("HiggsTools") and No. PITN-GA-2012-315877 ("MCnetITN"), and by the ERC Advanced Grant MC@NNLO (No. 340983).

[1] W. Beenakker, S. Dittmaier, M. Kramer, B. Plumper, M. Spira, and P. M. Zerwas, Higgs Radiation off Top Quarks at the Tevatron and the LHC, Phys. Rev. Lett. **87**, 201805 (2001).

[2] W. Beenakker, S. Dittmaier, M. Kramer, B. Plumper, M. Spira, and P. M. Zerwas, NLO QCD corrections to t anti-t H production in hadron collisions, Nucl. Phys. **B653**, 151 (2003).

[3] S. Dawson, L. H. Orr, L. Reina, and D. Wackeroth, Associated top quark Higgs boson production at the LHC, Phys. Rev. D **67**, 071503 (2003).

[4] S. Dawson, C. Jackson, L. H. Orr, L. Reina, and D. Wackeroth, Associated Higgs production with top quarks at the large hadron collider: NLO QCD corrections, Phys. Rev. D **68**, 034022 (2003).

[5] A. Bredenstein, A. Denner, S. Dittmaier, and S. Pozzorini, NLO QCD Corrections to pp $pp \to t\bar{t}b\bar{b} + X$ at the LHC, Phys. Rev. Lett. **103**, 012002 (2009).

[6] A. Bredenstein, A. Denner, S. Dittmaier, and S. Pozzorini, NLO QCD Corrections to Top Anti-Top Bottom Anti-Bottom Production at the LHC: 2. full hadronic results, J. High Energy Phys. 03 (2010) 021.

[7] F. Cascioli, P. Maierhofer, and S. Pozzorini, Scattering Amplitudes with Open Loops, Phys. Rev. Lett. **108**, 111601 (2012).

[8] T. Gleisberg, S. Hoeche, F. Krauss, A. Schalicke, S. Schumann, and J.-C. Winter, SHERPA 1. alpha: A Proof of concept version., J. High Energy Phys. 02 (2004) 056.

[9] T. Gleisberg, S. Hoeche, F. Krauss, M. Schonherr, S. Schumann, F. Siegert, and J. Winter, Event generation with SHERPA 1.1, J. High Energy Phys. 02 (2009) 007.

[10] J. Alwall, M. Herquet, F. Maltoni, O. Mattelaer, and T. Stelzer, MadGraph 5: Going beyond, J. High Energy Phys. 06 (2011) 128.

[11] J. Alwall, R. Frederix, S. Frixione, V. Hirschi, F. Maltoni, O. Mattelaer, H. S. Shao, T. Stelzer, P. Torrielli, and M. Zaro, The automated computation of tree-level and next-to-leading order differential cross sections, and their matching to parton shower simulations, J. High Energy Phys. 07 (2014) 079.

[12] S. Frixione and B. R. Webber, Matching NLO QCD computations and parton shower simulations, J. High Energy Phys. 06 (2002) 029.

[13] R. Frederix, S. Frixione, V. Hirschi, F. Maltoni, R. Pittau, and P. Torrielli, Scalar and pseudoscalar Higgs production in association with a topantitop pair, Phys. Lett. B **701**, 427 (2011).

[14] F. Cascioli, P. Maierhöfer, N. Moretti, S. Pozzorini, and F. Siegert, NLO matching for $t\bar{t}b\bar{b}$ production with massive $b$-quarks, Phys. Lett. B **734**, 210 (2014).

[15] S. Hoeche, F. Krauss, M. Schonherr, and F. Siegert, QCD matrix elements + parton showers: The NLO case, J. High Energy Phys. 04 (2013) 027.

[16] R. Frederix and S. Frixione, Merging meets matching in MC@NLO, J. High Energy Phys. 12 (2012) 061.

[17] L. Lonnblad and S. Prestel, Unitarising matrix element + parton shower merging, J. High Energy Phys. 02 (2013) 094.

[18] S. Plätzer, Controlling inclusive cross sections in parton shower + matrix element merging, J. High Energy Phys. 08 (2013) 114.

[19] S. Hoeche, J. Huang, G. Luisoni, M. Schoenherr, and J. Winter, Zero and one jet combined next-to-leading order analysis of the top quark forward-backward asymmetry, Phys. Rev. D **88**, 014040 (2013).

[20] S. Hoeche, F. Krauss, P. Maierhoefer, S. Pozzorini, M. Schonherr, and F. Siegert, Next-to-leading order QCD predictions for top-quark pair production with up to two jets merged with a parton shower, Phys. Lett. B **748**, 74 (2015).

[21] V. Khachatryan *et al.* Search for a Standard Model Higgs boson produced in association with a top-quark pair and decaying to bottom quarks using a matrix element method, Eur. Phys. J. C **75**, 251 (2015).

[22] G. Aad *et al.*, Search for the Standard Model Higgs boson produced in association with top quarks and decaying into $b\bar{b}$ in pp collisions at $\sqrt{s} = 8$ TeV with the ATLAS detector, Eur. Phys. J. C **75**, 349 (2015).

[23] N. Moretti, P. Petrov, S. Pozzorini, and M. Spannowsky, Measuring the signal strength in ttH with H- > bb (to be published).

[24] M. R. Buckley and D. Goncalves, Boosting the direct $CP$ measurement of the Higgs-top coupling (to be published).

[25] G. Aad *et al.*, Performance of $b$-Jet identification in the ATLAS experiment (to be published).

[26] The ATLAS collaboration, Commissioning of the ATLAS high-performance $b$-tagging algorithms in the 7 TeV collision data, Technical Report No. ATLAS-CONF-2011-102, CERN, Geneva, 2011.

[27] S. Chatrchyan *et al.* (The CMS collaboration), Identification of b-quark jets with the cms experiment, J. Instrum. **8**, P04013 (2013).

[28] G. Piacquadio and C. Weiser, A new inclusive secondary vertex algorithm for b-jet tagging in atlas, J. Phys. Conf. Ser. **119**, 032032 (2008).

[29] P. Abreu *et al.*, Measurement of the multiplicity of gluons splitting to bottom quark pairs in hadronic $Z^0$ decays, Phys. Lett. B **405**, 202 (1997).

[30] R. Barate *et al.*, A measurement of the gluon splitting rate into $b\bar{b}$ pairs in hadronic Z decays, Phys. Lett. B **434**, 437 (1998).

[31] P. Abreu *et al.*, Measurement of the rate of $b\bar{b}b\bar{b}$ events in hadronic Z decays and the extraction of the gluon splitting into $b\bar{b}$, Phys. Lett. B **462**, 425 (1999).

[32] G. Abbiendi *et al.*, Production rates of $b\bar{b}$ quark pairs from gluons and $b\bar{b}b\bar{b}$ events in hadronic $Z^0$ decays, Eur. Phys. J. C **18**, 447 (2001).

[33] D. Acosta *et al.*, Measurements of $b\bar{b}$ azimuthal production correlations in $p\bar{p}$ collisions at $\sqrt{s} = 1.8$ TeV, Phys. Rev. D **71**, 092001 (2005).

[34] The ATLAS collaboration, Identification and tagging of double $b$ -hadron jets with the ATLAS detector, Technical Report No. ATLAS-CONF-2012-100, CERN, Geneva, 2012.

[35] $b$-tagging in boosted topologies (to be published).

[36] M. Bahr *et al.* Herwig++ physics and manual, Eur. Phys. J. C **58**, 639 (2008).

[37] T. Sjöstrand, S. Ask, J. R. Christiansen, R. Corke, N. Desai, P. Ilten, S. Mrenna, S. Prestel, C. O. Rasmussen, and P. Z. Skands, An Introduction to PYTHIA 8.2., Comput. Phys. Commun. **191**, 159 (2015).

[38] J. Gallicchio and M. D. Schwartz, Quark and Gluon Tagging at the LHC, Phys. Rev. Lett. **107**, 172001 (2011).

[39] J. Gallicchio and M. D. Schwartz, Quark and gluon jet substructure, J. High Energy Phys. 04 (2013) 090.

[40] S. Schumann and F. Krauss, A parton shower algorithm based on Catani-Seymour dipole factorization, J. High Energy Phys. 03 (2008) 038.

[41] A. Buckley, J. Butterworth, L. Lonnblad, D. Grellscheid, H. Hoeth, J. Monk, H. Schulz, and F. Siegert, Rivet user manual, Comput. Phys. Commun. **184**, 2803 (2013).

[42] M. Cacciari, G. P. Salam, and G. Soyez, The anti-$k_t$ jet clustering algorithm, J. High Energy Phys. 04 (2008) 063.